***Xenopus* embryo and oocyte microinjection.** hWIF-1 was expressed from the pCS2$^+$ expression vector. RNA synthesis and microinjection into *Xenopus* embryos have been described[15].

Armadillo stabilization assays. *Drosophila* clone-8 cells, seeded one day earlier and grown to 80% confluence, were incubated with control or Wg-containing conditioned medium from S2 cells. Before incubation with clone-8 cells, the S2 conditioned medium (0.4 ml) was pre-incubated for 25 min at 4 °C with 0.4 ml DMEM/F-12 medium from transfected or control 293 cells. After 3 h at 25 °C, clone-8 cells were collected, washed in 1 × PBS, 5 mM EDTA, and lysed in 80 μl hypotonic buffer (10 mM Tris, pH 7.5, 0.2 mM $MgCl_2$) containing protease inhibitors. After addition of 20 μl 1.25 M sucrose, a membrane-free cytoplasmic fraction was prepared by centrifugation at 100,000*g* for 30 min at 4 °C, resolved by SDS–PAGE, immunoblotted and analysed for Armadillo (mAb N2-7A1; ref. 16), actin (Amersham) and HSP-70 (Sigma).

Solution binding assay for Wg and XWnt8–Myc. 200 μl 293-cell conditioned medium containing WIF-1–IgG, WD–IgG, or IgG (each adjusted by ultrafiltration to 60 nM) was incubated with protein A–Sepharose beads at 4 °C for 1 h, after which the beads were washed 3 times with PBS and then incubated with 400 μl Wg or XWnt8–Myc conditioned medium at 4 °C for 2 h. The beads were separated from unbound material by low-speed centrifugation and washed five times with PBS. Co-precipitates were analysed by SDS–PAGE and immunoblotted with affinity-purified rabbit anti-Wg antibodies or anti-Myc mAb 9E10 (ref. 17).

Quantitative binding of XWnt8–AP and hWIF-1. Conditioned medium (100 μl) containing WIF-1 (10 μg ml^{-1}), WIF-1–IgG (5 μg ml^{-1}), or IgG (4 μg ml^{-1}) was used to coat 96-well plate at 4 °C overnight, followed by incubation at 4 °C for 4 h with 200 μl 2 mg ml^{-1} BSA in binding buffer (Hank's balanced salt, 20 mM HEPES, pH 7.0). 150 μl XWnt8–AP diluted in 2 mg ml^{-1} BSA in binding buffer was applied to each well and incubated at 4 °C for 24 h. After 5 washes with 200 μl each of binding buffer, bound XWnt8–AP was quantified by measuring alkaline phosphatase activity spectrophotometrically. A plot of alkaline phosphatase activity, representing the concentration of bound XWnt8–AP relative to the total concentration of XWnt8, was fitted to the simple binary binding model ($A + B \leftrightarrow A{\cdot}B$).

Received 17 December 1998; accepted 26 January 1999.

1. Wodarz, A. & Nusse, R. Mechanisms of Wnt signaling in development. *Annu. Rev. Cell Dev. Biol.* **14,** 59–88 (1998).
2. Moon, R. T., Brown, J. D. & Torres, M. WNTs modulate cell fate and behavior during vertebrate development. *Trends Genet.* **13,** 157–162 (1997).
3. Glinka, A. *et al.* Dickkopf-1 is a member of a new family of secreted proteins and functions in head induction. *Nature* **391,** 357–362 (1998).
4. Hoppler, S., Brown, J. D. & Moon, R. T. Expression of a dominant-negative Wnt blocks induction of MyoD in *Xenopus* embryos. *Genes Dev.* **10,** 2805–2817 (1996).
5. Christian, J. L. & Moon, R. T. Interactions between XWnt-8 and Spemann organizer signaling pathways generate dorsoventral pattern in the embryonic mesoderm of *Xenopus*. *Genes Dev.* **7,** 13–28 (1993).
6. Moon, R. T. *et al.* Dissecting Wnt signaling pathways and Wnt-sensitive developmental processes through transient misexpression analyses in embryos of *Xenopus laevis*. *Development* (suppl.), 85–94 (1993).
7. van Leeuwen, F., Harryman Samos, C. & Nusse, R. Biological activity of soluble Wingless protein in cultured *Drosophila* imaginal disc cells. *Nature* **368,** 342–344 (1994).
8. Piccolo, S., Sasai, Y., Lu, B. & DeRobertis, E. M. Dorsoventral patterning in *Xenopus*: inhibition of ventral signals by direct binding of chordin to BMP-4. *Cell* **86,** 589–598 (1996).
9. Zimmerman, L. B., De Jesus-Escobar, J. M. & Harland, R. M. The Spemann organizer signal noggin binds and inactivates bone morphogenetic protein 4. *Cell* **86,** 599–606 (1996).
10. Hsu, D. R., Economides, A. N., Wang, X., Eimon, P. M. & Harland, R. M. The *Xenopus* dorsalizing factor gremlin identifies a novel family of secreted proteins that antagonize BMP activities. *Mol. Cell* **1,** 673–683 (1998).
11. Cadigan, K. M., Fish, M. P., Rulifson, E. J. & Nusse, R. Wingless repression of *Drosophila frizzled2* expression shapes the Wingless morphogen gradient. *Cell* **93,** 767–777 (1998).
12. Finch, P. W. *et al.* Purification and molecular cloning of a secreted frizzled-related antagonist of Wnt signaling. *Proc. Natl Acad. Sci. USA* **94,** 6770–6775 (1997).
13. Aruffo, A., Stamenkovic, I., Melnick, M., Underhill, C. B. & Seed, B. CD44 is the principal cell surface receptor for hyaluronate. *Cell* **61,** 1303–1313 (1990).
14. Rebagliati, M. R., Toyoma, R., Haffter, P. & Dawid, I. B. Cyclops encodes a nodal-related factor involved in midline signaling. *Proc. Natl Acad. Sci. USA* **95,** 9932–9937 (1998).
15. He, X., Saint-Jeannet, J.-P., Woodgett, J. R., Varmus, H. E. & Dawid, I. B. Glycogen synthase kinase-3 and dorsoventral patterning in *Xenopus* embryos. *Nature* **374,** 617–622 (1995).
16. Peifer, M., Orsulic, S., Sweeton, D. & Wieschaus, E. A role for the *Drosophila* segment polarity gene *armadillo* in cell adhesion and cytoskeletal integrity during oogenesis. *Development* **118,** 1191–1207 (1993).
17. Evan, G. I., Lewis, G. K., Ramsay, G. & Bishop, M. J. Isolation of monoclonal antibodies specific for human c-*myc* proto-oncogene product. *Mol. Cell. Biol.* **5,** 3610–3616 (1985).

Acknowledgements. We thank R. Moon for Xwnt8-Myc cDNA, J. Flanagan for the alkaline phosphatase plasmid, J. Corden for the mouse RNA polymerase II clone, B. Appel, L. Roman and D. Grunwald for cDNA libraries, and P. Bhanot and I. Munoz-Sanjuan for comments on the manuscript. Supported by the Howard Hughes Medical Institute (J.-C.H., A.R., P.M.S., C.H.S., R.N., J.N.).

Correspondence and requests for materials should be addressed to J.N. (e-mail: jnathans@jhmi.edu). Genbank accession numbers for WIF-1 are: human, AF122922; mouse, AF122923; *Xenopus*, AF122924; zebrafish, AF122925.

A capsaicin-receptor homologue with a high threshold for noxious heat

Michael J. Caterina*, Tobias A. Rosen*†, Makoto Tominaga*†, Anthony J. Brake* & David Julius*

** Department of Cellular and Molecular Pharmacology, University of California, San Francisco, California 94143-0450, USA*

† These authors contributed equally to this work

Pain-producing heat is detected by several classes of nociceptive sensory neuron that differ in their thermal response thresholds[1–3]. The cloned capsaicin receptor, also known as the vanilloid receptor subtype 1 (VR1), is a heat-gated ion channel that has been proposed to mediate responses of small-diameter sensory neurons to moderate (43 °C) thermal stimuli[4,5]. VR1 is also activated by protons, indicating that it may participate in the detection of noxious thermal and chemical stimuli *in vivo*. Here we identify a structurally related receptor, VRL-1, that does not respond to capsaicin, acid or moderate heat. Instead, VRL-1 is activated by high temperatures, with a threshold of ~52 °C. Within sensory ganglia, VRL-1 is most prominently expressed by a subset of medium- to large-diameter neurons, making it a candidate receptor for transducing high-threshold heat responses in this class of cells. VRL-1 transcripts are not restricted to the sensory nervous system, indicating that this channel may be activated by stimuli other than heat. We propose that responses to noxious heat involve these related, but distinct, ion-channel subtypes that together detect a range of stimulus intensities.

To identify new proteins involved in the detection of noxious stimuli by sensory neurons, we searched the GenBank database for sequences related to VR1. Most of the expressed sequence tag (EST) sequences identified appeared to encode human and mouse orthologues of the same protein, which we named vanilloid-receptor-like protein 1 (VRL-1). Using this information we isolated full-length VRL-1 complementary DNAs from rat brain and the CCRF-CEM human myeloid cell line (Fig. 1). These clones encode proteins of 761 amino acids and 764 amino acids, respectively, which share 78.4% identity and 86.2% similarity with one another. By comparison, rat and human VRL-1 are roughly 49% identical and 66% similar to rat VR1.

Like VR1, VRL-1 is predicted to contain six transmembrane domains, a putative pore-loop region, a cytoplasmic amino terminus with three ankyrin-repeat domains, and a cytoplasmic carboxy terminus. This overall architecture is characteristic of a family of ion channels defined by the transient receptor potential (TRP) and TRP-like (TRPL) channels of the *Drosophila* phototransduction pathway and which is now known to include vertebrate and nematode homologues[6–8]. Of the TRP-related sequences reported so far, the one that resembles VR1 and VRL-1 most closely is that of the OSM-9 protein, which is required for osmosensation and the detection of some odorants in *Caenorhabditis elegans*[8]. Even OSM-9, however, is only 23% identical to rat VR1 and 24% identical to rat VRL-1, indicating that these latter molecules may form a distinct subgroup within this growing family of proteins.

VR1 is activated by capsaicin (the main pungent ingredient in 'hot' chilli peppers) and by its very potent analogue, resiniferatoxin (from *Euphorbia* plants). These vanilloid compounds elicit pain by evoking non-selective cationic currents in small-diameter nociceptive neurons (nociceptors)[4,9–11]. Even at very high concentrations, however, neither capsaicin (Fig. 2a, d) nor resiniferatoxin (not shown) evoked currents in *Xenopus* oocytes or HEK293 human embryonic kidney cells expressing VRL-1. Thus, VRL-1 does not

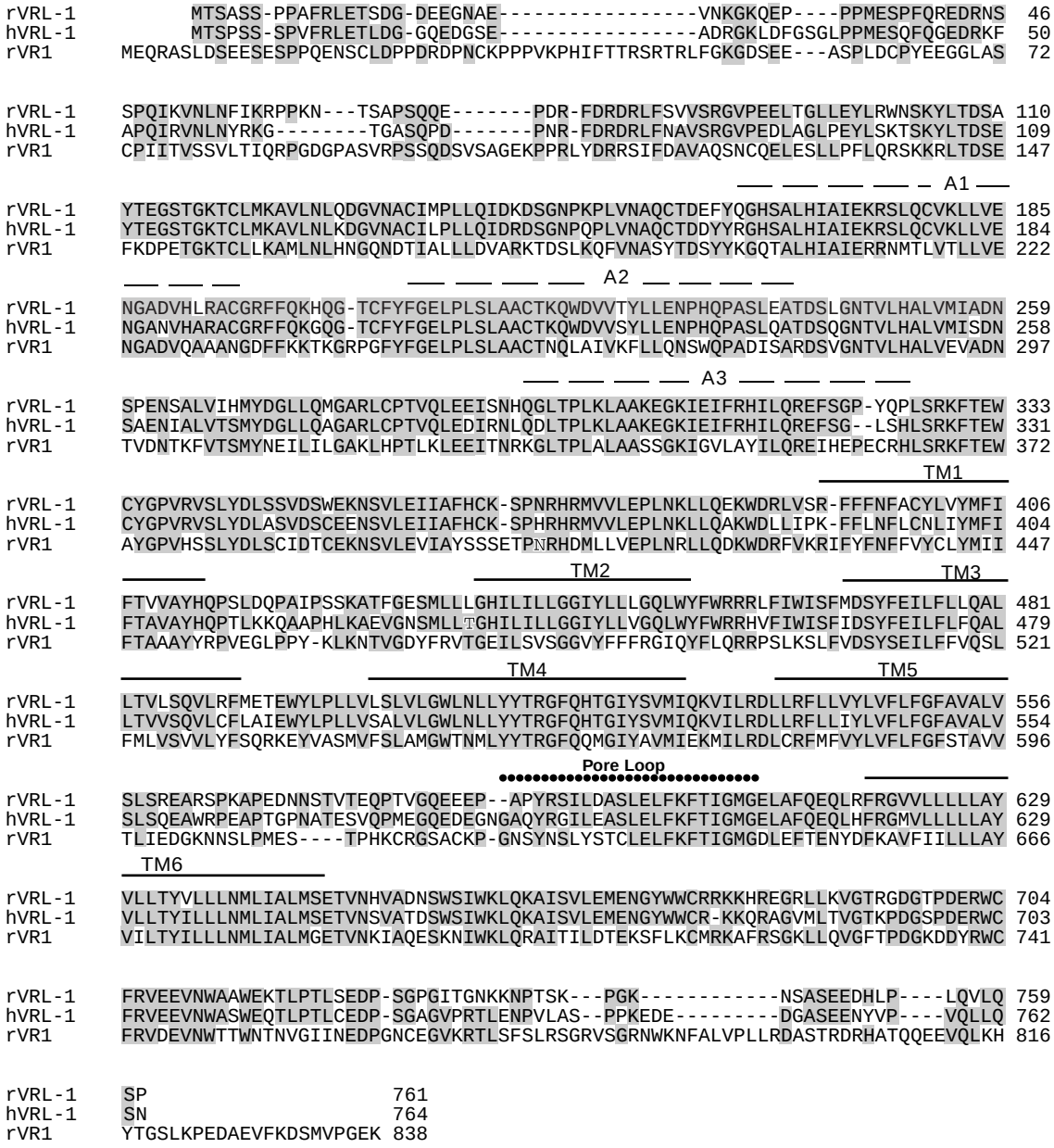

Figure 1 Alignment of cDNA sequences of rat VRL-1, human VRL-1 and rat VR1. Ankyrin-repeat domains (dashed black lines), putative transmembrane (TM) domains (solid black lines) and the pore-loop region (dotted black line) are indicated. Identical residues are shaded in grey.

appear to be a vanilloid receptor. VR1 can also be activated by low pH (<pH 6.0) or by thermal stimuli sufficient to cause pain in mammals (>43 °C)[4,5]. We therefore investigated whether protons or heat could evoke currents in HEK293 cells or oocytes expressing VRL-1. Bath acidification to pH 4.0 did not produce responses in either system, and neither did temperature increases in the low-to-moderate noxious range (<50 °C). We did, however, observe pronounced currents when bath temperatures were raised from 22 °C to >53 °C (Fig. 2a, d). These responses, seen in 15 out of 20 batches of VRL1-injected oocytes and in ~70% of VRL1-transfected HEK293 cells, were markedly larger than the background heat-evoked currents observed in control water-injected oocytes or vector-transfected HEK293 cells, indicating that they may be mediated by VRL-1. No such currents were observed in oocytes injected with complementary RNA encoding the $5HT_3$ serotonin receptor, or in HEK293 cells expressing the $P2X_2$ ATP receptor (not shown).

Having identified a stimulus for VRL-1, we asked whether this channel shares pharmacological or electrophysiological properties in common with VR1. Capsazepine (10 μM), a competitive antagonist that blocks vanilloid-, proton-, or heat-evoked responses in VR1-expressing cells[4,5,12], had no effect on heat-evoked currents in VRL1-expressing oocytes (not shown). In contrast, the non-competitive VR1 antagonist ruthenium red[4,5,13] inhibited heat-evoked VRL-1 responses significantly (90.1 ± 5% at 10 μM, mean ± s.d.) and dose dependently (half-maximal inhibitory concentration = 0.62 μM, Fig. 2b, c). The current–voltage relationship of heat-evoked VRL-1 responses in transfected HEK293 cells showed dual rectification, with a more prominent outward component (Fig. 2e). Although VR1-mediated currents exhibit only outward rectification at both whole-cell and single-channel levels[4,5], rectification of VRL-1 more closely resembles that seen for the *Drosophila* TRP channel[14]. Currents mediated by VRL-1 are cationic, with a permeability sequence $Ca^{2+} > Mg^{2+} > Na^{+} \approx Cs^{+} \approx K^{+}$, and relative permeability ratios (Fig. 2f) similar to those for heat-evoked currents in VR1-expressing cells[5]. This functional similarity may reflect the

sequence conservation within the putative pore regions of these two proteins (Fig. 1).

Single-unit recordings from peripheral nerves have shown that heat-sensitive nociceptors can be subdivided into medium- and high-threshold classes, depending on whether they fire when temperatures exceed ~43 °C or ~53 °C, respectively[1–3]. The threshold for VR1 activation is ~43 °C in transfected HEK293 cells (Fig. 3a, middle tracing)[5]. In contrast, heat-evoked currents in VRL1-expressing HEK293 cells did not develop until the bath temperature exceeded 50 °C (Fig. 3a, top tracing). A more detailed thermal response profile generated at a series of plateaux bath temperatures yielded a threshold value for VRL-1 activation of 50–52 °C, compared with the lower activation threshold of ~44 °C for VR1 (Fig. 3b). When VR1 and VRL-1 were co-expressed in HEK293 cells, a bimodal heat-evoked current was observed that appeared to represent the addition of a desensitizing medium-threshold VR1 response and a high-threshold VRL-1 response (Fig. 3a, bottom tracing). These findings indicate that VR1 and VRL-1 channels can account for responses of medium- and high-threshold nociceptors, respectively, to heat.

When temperature ramps were applied to oocytes expressing VR1 or VRL-1, initial heat-evoked currents developed at about 45 °C or 53 °C, respectively (Fig. 3c, d), again showing that these two channel subtypes have distinct thresholds for heat activation. These continuous thermal-response profiles also illustrate the extremely steep temperature dependence of the currents once threshold is reached. In the oocyte system, the thermal sensitivities of both VR1 and VRL-1 increased with repeated heat applications (Figs 2b, 3d); by the second or third stimulus, either channel could be activated by temperatures as low as 40 °C. This pattern of sensitization resembles

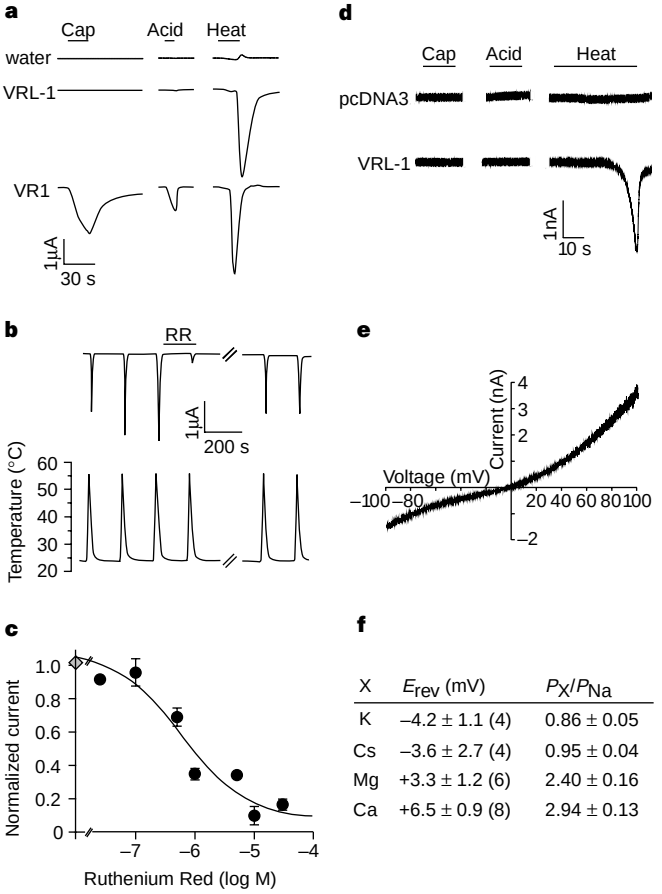

X	E_{rev} (mV)	P_X/P_{Na}
K	–4.2 ± 1.1 (4)	0.86 ± 0.05
Cs	–3.6 ± 2.7 (4)	0.95 ± 0.04
Mg	+3.3 ± 1.2 (6)	2.40 ± 0.16
Ca	+6.5 ± 0.9 (8)	2.94 ± 0.13

Figure 2 VRL-1 is activated by heat, but not by vanilloids or protons. **a**, Voltage-clamp analysis of oocytes injected with water (top), VRL-1 cRNA (middle), or VR1 cRNA (bottom). Oocytes were exposed to capsaicin (1 μM), protons (pH 4) or heat (23 °C to 55 °C in 15 s). Duration of heat stimuli varied by ~3 s between experiments, but peak temperatures were within ±0.4 °C of each other. Capsaicin (100 μM), resiniferatoxin (10 μM), ATP (100 μM), acetylcholine (300 μM), histamine (10 μM), substance P (1 μM), bradykinin (1 μM) and serotonin (10 μM) did not evoke currents in VRL1-injected oocytes (not shown). **b**, Ruthenium red (RR, 10 μM) reversibly inhibits heat-evoked currents in oocytes expressing VRL-1. The wash-out period (starting parallel lines) was 10 min. **c**, Dose dependence of RR-mediated inhibition of heat-evoked (54 °C) currents in oocytes expressing VRL-1. Current magnitudes were normalized to that of the third heat response in a given oocyte. Mean values (±s.e.m., n = 4–6 oocytes per point) were fitted to the Hill equation. In oocytes not treated with RR, the fourth heat-evoked response was the same as the third (1.01 ± 0.03-fold, diamond). **d**, Whole-cell voltage-clamp analysis of HEK293 cells transfected with vector (pcDNA3) or VRL-1 cDNA. Cells were successively exposed to capsaicin (100 μM), protons (pH 4) and heat (22 °C to 54 °C in 45 s). Resiniferatoxin (1 μM) evoked no current in VRL1-expressing cells (not shown). **e**, Current–voltage relationship for heat-evoked currents in VRL1-transfected HEK293 cells. A voltage ramp was applied from –100 mV to +100 mV in 500 ms. The reversal potential (E_{rev}), obtained with caesium aspartate pipette solution, was −3.1 ± 0.5 mV (n = 10). **f**, Relative cationic permeabilities (P_X/P_{Na}) of heat-evoked currents in VRL1-transfected HEK293 cells. Values shown are means ± s.e.m. (number of independent cells).

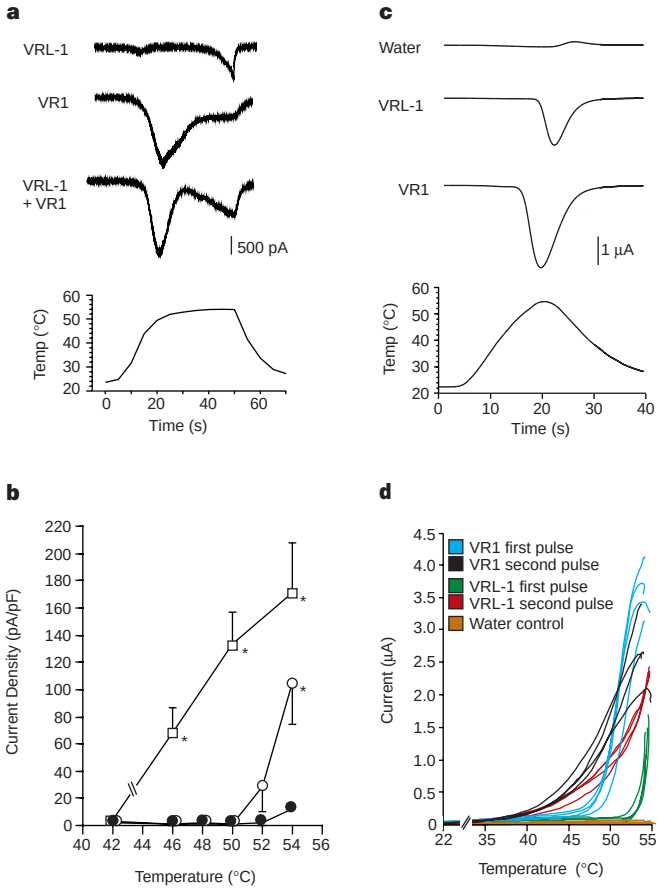

Figure 3 VRL-1 exhibits a higher activation threshold than VR1. **a**, Currents evoked by temperature ramps in HEK293 cells expressing VRL-1 (top), VR1 (middle), or both (bottom). Bath temperature is plotted below (final temperature 54 °C). **b**, Temperature-response profile of heat-evoked currents in HEK293 cells transfected with pcDNA3 (filled circles), VR1 (squares) or VRL-1 (open circles) plasmids. Asterisks indicate significant differences from pcDNA3 ($P < 0.01$, unpaired Student's t-test) (pcDNA3, n = 5; VR1, n = 7; VRL-1, n = 24). **c**, Currents evoked by a temperature ramp in oocytes injected with water or VRL-1 or VR1 cRNA. **d**, Response profiles of four oocytes exposed to two successive heat ramps, as in **c**.

that exhibited by some nociceptors following an initial exposure to noxious heat[2]. We also subjected VRL1-expressing oocytes to two consecutive subthreshold heating cycles (23 °C to 50 °C), followed by a cycle spanning 23 °C to 56 °C. In this case, currents were observed only in the third cycle, after the temperature exceeded 53 °C (not shown), showing that the higher threshold observed for VRL-1 does not reflect simply a latent response to a lower threshold temperature. Moreover, these results show that subthreshold temperatures do not sensitize VRL-1.

Thermally responsive nociceptors differ not only in their activation thresholds, but also with respect to size and myelination pattern[15]. C-polymodal nociceptors are small-diameter, unmyelinated neurons that respond to heat with a threshold of ~43 °C. Aδ mechano- and heat-sensitive (AMH) neurons are medium- to large-diameter, lightly myelinated neurons that fall into two groups: type I AMHs have a response threshold of ~53 °C, and type II AMHs are activated at ~43 °C (refs 1, 3, 15). We therefore used VR1- and VRL1-specific antisera to determine whether the distribution of these two receptors within sensory ganglia shows a correlation with these cells types. In rat dorsal root ganglia (DRG), VR1 expression was observed in 40% of all neurons (157 out of 397), predominantly in a population with small cell bodies (19.2 ± 0.3 μm, mean diameter ± s.e.m.; Figs 4a, 5 top). This observation is consistent with previous histological and functional studies[4,5,16–18].

Intense VRL-1 immunoreactivity was observed in 16.4% of all DRG neurons (152/925) (arrowheads in Fig. 4b), and an analysis of size distribution showed that these cells were of medium to large diameter (29.0 ± 0.6 μm, mean diameter ± s.e.m.; Fig. 5, bottom). More moderate VRL-1 immunoreactivity was seen in neurons with very large diameters, where staining was confined to the plasma membrane (arrows in Fig. 4b). Similar expression profiles were observed in trigeminal ganglia (not shown). Very few of the intensely VRL1-positive cells stained with lectin IB4 (1/58, Fig. 4c) or substance P antibody (3/57, not shown), markers for two populations of small-diameter nociceptive neurons[19]. However, about one-third of the intensely VRL1-positive cells (41/114) co-stained with antiserum against CGRP (arrows in Fig. 4e, f), consistent with the expression pattern reported for rat Aδ neurons[20].

Distinct distributions of VR1 and VRL-1 were also observed in primary cultures of rat DRG neurons (not shown). Roughly 80% of VRL1-immunoreactive cells (85/105) in these cultures stained with the anti-neurofilament antibody RT97 (Fig. 4d), a marker for myelinated neurons[21,22]. Within the spinal cord, intense VRL-1 immunoreactivity was observed in Lissauer's tract and in the dorsal horn (Fig. 4g). Dorsal horn staining was most intense within the marginal zone and lamina I (Fig. 4g, arrowhead), as well as in a band spanning the boarder between inner lamina II and lamina III (Fig. 4g, arrow). This pattern, confirmed by double labelling with IB4 (not shown), resembles that formed by central terminals of Aδ primary afferents[23], although a contribution from intrinsic dorsal horn neurons cannot be excluded. VRL-1 immunoreactivity was also seen in the dorsal columns (consistent with the lower-level immunoreactivity observed in large-diameter DRG neurons), in motoneurons and in astrocytes (not shown).

These histological results, together with the temperature-response data, indicate that robust expression of VRL-1 by a group of Aδ neurons may underlie the characteristically high thermal threshold ascribed to type I AMH nociceptors. Expression of VR1 by C-nociceptors could account for the moderate thermal threshold exhibited by these neurons. This proposal is in agreement with the results of a recent electrophysiological study[24] that showed that cultured sensory neurons fall into two classes with regard to heat sensitivity: low-threshold (45 °C), capsaicin-responsive cells with small diameters (~19 μm) and high-threshold (51 °C), capsaicin-insensitive cells with larger diameters (~26 μm). Finally, we found that VRL-1 messenger RNA is expressed in tissues other than sensory ganglia and spinal cord, including lung, spleen, intestine, and brain (most subregions) (Fig. 4h, and data not shown). In these locations, VRL-1 may be activated by stimuli other than noxious heat.

Genetic analyses in invertebrate systems have placed TRP and related proteins downstream of G-protein-coupled signalling cascades, most notably in pathways involving the hydrolysis of mem-

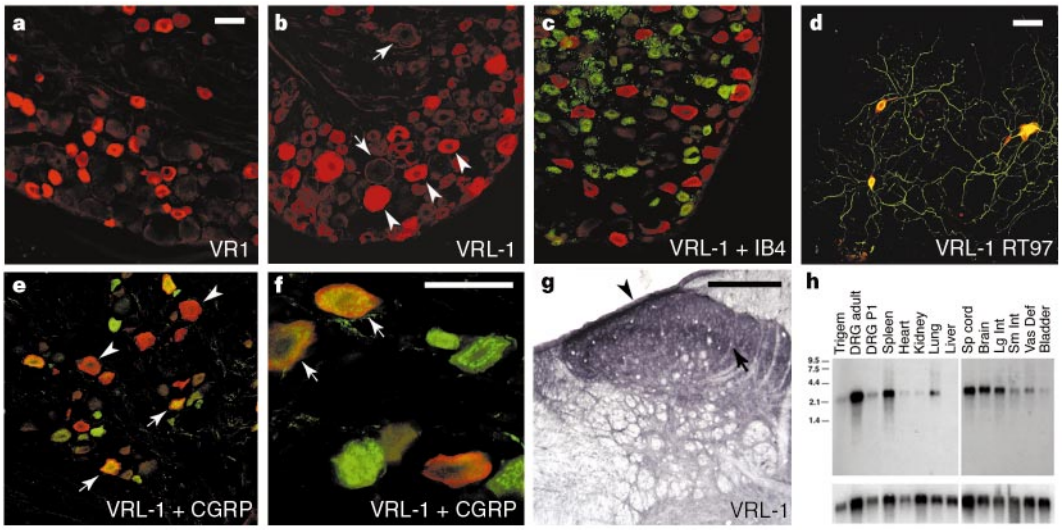

Figure 4 VRL-1 is highly expressed in a subset of medium- to large-diameter sensory neurons. Rat DRG sections (15 μm) were stained with: **a**, anti-VR1; **b**, anti-VRL1; **c**, anti-VRL1 (red) plus FITC–lectin IB4 (green); **e**, **f**, anti-VRL1 (red) and anti-CGRP (green) antibodies. **d**, Cultured sensory neurons stained with anti-VRL1 (red) and RT97 anti-neurofilament (green) antibodies. Double staining appears yellow. **g**, Spinal cord sections stained with anti-VRL1 antibody. **h**, Northern blot analysis of VRL-1 mRNA expression in rat tissues. Blots were probed with VRL-1 cDNA (top), and with rat cyclophilin cDNA (bottom) to normalize for loading. DRG P1 indicates neonatal DRG. Molecular-size markers (in kilobases) are shown at the left. Scale bar in **a** (50 μm) also applies to **b**, **c**, **e**. Scale bars in **d**, **f**, **g** represent 100, 50, and 200 μm, respectively. In **b**, arrowheads indicate intense staining of medium- to large-diameter neurons, and arrows indicate staining of neurons with very large diameters. In **e**, **f**, arrows and arrowheads indicate double- (yellow) and single-positive cells, respectively. VRL-1 peptide, but not control peptide, greatly diminished VRL-1 staining (not shown).

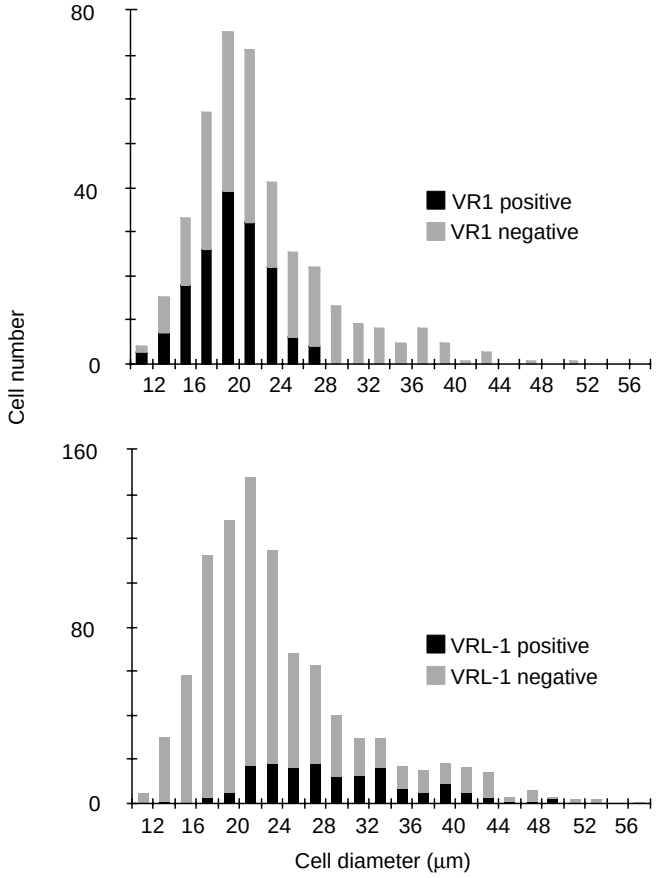

Figure 5 VR1 and VRL-1 proteins show distinct expression patterns among DRG neurons of different size classes. Only intensely labelled cells were counted as positive.

brane lipids[25,26]. We found VRL-1 transcripts in many non-neuronal tissues. As these tissues are unlikely to encounter temperatures above 50 °C, other physiological stimuli might regulate the channel at these sites, either directly or through the release of (perhaps G-protein-mediated) second messengers. The thermal-response characteristics of VRL-1 might also be controlled by such mechanisms. Nevertheless, the observation that VR1 and VRL-1 exhibit distinct thresholds for activation by heat indicates that their absolute thermal sensitivities may be governed, at least in part, by their primary sequences.

Individual members of receptor-protein families are often tuned to detect a stimulus over a discrete window of intensities. Together, an ensemble of such receptor subtypes can recognize a physiological stimulus over a wide dynamic range. Perhaps the best example of such a strategy is provided by the vertebrate visual system[27], where different opsin subtypes are tuned to discrete frequency ranges of the electromagnetic spectrum. By analogy, our findings indicate that related ion channels may account for thermal responsiveness over a range of noxious temperatures. In addition to its ability to sense noxious heat, the nervous system is responsive to a broad range of noxious and innocuous temperatures, from warm to cold. It will therefore be interesting to determine the extent to which vanilloid receptor-like subtypes contribute to this sensory repertoire. □

Methods

Molecular biology. Polymerase chain reaction (PCR) primers (5′-GACCA GCAAGTACCTCAC-3′ and 5′-CTCCCATGCAGCCCAGTTTACTTCCACCC TGAAGCACCAGCGCTCA-3′) were designed from VR1-related EST sequences and used to amplify a 1,985-nucleotide fragment from neonatal rat brain as described[28]. A full-length rat VRL-1 cDNA containing a 2,283-nucleotide open reading frame with 5′ and 3′ untranslated regions of 329 and 105 nucleotides, respectively, was isolated from a rat brain cDNA plasmid library prepared as described[28]. Two other primers (5′-ATAAGAATGCGGCCGCGAGAGGTCCT GGCTGGAC-3′ and 5′-GGAAGATATCAGAGCCAGCAGTATGTGGTTG-3′) were used to amplify a full-length human VRL-1 cDNA from CCRF-CEM cells (a gift from J. Imboden).

Mammalian-cell electrophysiology. HEK293 cells were transfected using calcium phosphate with VR1 cDNA (diluted 1:200 with pcDNA3) or undiluted VRL-1 cDNA. In co-transfection experiments, VR1, VRL-1 and pcDNA3 plasmids were mixed at a ratio of 1:10:29 (total 12 μg DNA per 35-mm dish). For control experiments using $P2X_2$, cells were transfected with 1 μg of plasmid DNA using lipofectamine (Gibco). Whole-cell patch-clamp recordings were carried out as described[4]. Standard bath solution for whole-cell recordings contained (in mM): 140 NaCl, 5 KCl, 2 $MgCl_2$, 2 $CaCl_2$, 10 HEPES, 10 glucose, pH 7.4 (adjusted with NaOH). In some experiments, bath solution was buffered to pH 4.0 with 10 mM MES. For monovalent-cation substitution experiments, bath solution was changed to (in mM): 140 NaCl (or KCl or CsCl), 10 glucose and 10 HEPES (adjusted to pH 7.4 with NaOH, KOH or CsOH, respectively) and reversal potential was measured using voltage ramps (−100 to +40 mV in 500 ms). For divalent-cation substitution experiments, bath solution was changed to (in mM): 110 $MgCl_2$ (or $CaCl_2$), 2 $Mg(OH)_2$ (or $Ca(OH)_2$), 10 glucose, 10 HEPES, pH 7.4 (adjusted with HCl). Standard pipette solution contained (in mM): 140 CsCl (or 130 caesium aspartate and 10 NaCl for current–voltage analysis), 5 EGTA, 10 HEPES, pH 7.4 (adjusted with CsOH). Pipette solution for cation-substitution experiments contained (in mM): 140 NaCl, 10 HEPES, 5 EGTA, pH 7.4 (adjusted with NaOH). Bath temperature was raised by perfusion with preheated solutions and monitored using a thermocouple (Omega). For each heating protocol, averaged temperautre profiles were established during bath perfusion ($n \geq 5$) before cellular recording. Liquid-junction potentials (8.6–9.6 mV) were measured in separate experiments and corrections made for membrane potentials. Relative permeability ratios (P_X/P_{Na}) were calculated as described[4]. VRL1-transfected cells were defined as heat responsive if heat-evoked currents were greater than two standard deviations above the mean current observed in vector-transfected cells.

Oocyte electrophysiology. *Xenopus* oocytes were injected with 5–10 ng VR1, 25 ng VRL-1, or 25 ng $5HT_3$ cRNA, as described[4]. Two-electrode voltage-clamp analysis ($E_h = -40$ mV) was carried out 7–16 days post-injection. Recording solution contained (in mM): 90 NaCl, 1.0 KCl, 2.4 $NaHCO_3$, 0.1 $BaCl_2$, 1.0 $MgCl_2$, 10 HEPES, pH 7.6, unless otherwise indicated. Bath temperature was increased using an in-line solution heater (SH27A, Warner Instruments, Inc) and a timed relay. Chamber temperature was monitored (accuracy ±0.2 °C) with a Super MCJ thermocouple (Omega) placed within 2 mm of the oocyte. VRL1-injected oocyte batches were defined as heat responsive if more than half of the cells exhibited currents ≥ twofold those observed in water-injected oocytes. Roughly half of all VRL1-injected oocyte batches exhibited currents ≥ fivefold those exhibited by controls.

Localization of VRL-1 expression. Northern blot analysis was done using a ^{32}P-labelled fragment (nucleotides 381–2,299) of rat VRL-1 cDNA as described[28]. Rabbits were immunized (HTI, Inc.) with keyhole limpet haemacyanin-conjugated peptide corresponding to the C terminus of rat VRL-1 plus an N-terminal cysteine (peptide sequence CKNSASEEDHLPLQVLQSP). Affinity purification of the antiserum was done after coupling the peptide to amine-reactive resin (Pierce). The antiserum specifically recognized a band of relative molecular mass ~80,000 (M_r ~80K) in whole-cell extracts prepared from HEK293 cells transfected with rat VRL-1 cDNA (not shown). For peptide competition, diluted antibody solutions (5 μg ml^{-1}) were preincubated (4 °C, 60 min) with 5–20 μg ml^{-1} VRL1-antigenic peptide or control peptide (CEDAEVFKDSMVPGEK).

Fixed frozen sections from adult rat sensory ganglia (15 μm) and spinal cord (35 μm) were prepared as described[5]. Immunofluorescence was performed as described[5] using rabbit anti-VRL1 (0.83 μg ml^{-1}), rabbit anti-VR1 (0.5 μg ml^{-1}), fluorescein isothiocyanate (FITC)-conjugated lectin IB4 (8 μg ml^{-1}, Sigma) guinea pig anti-substance P (1:12,000; Peninsula), guinea pig anti-CGRP (1:200, Peninsula), mouse monoclonal RT97 antibodies (10 μg ml^{-1}, Boehringer), and/or mouse anti-NeuN (1:3,000; Chemicon),

followed by Cy3-labelled goat anti-rabbit (1:700; Jackson Immunoresearch), Cy2-labelled donkey anti-guinea-pig (1:100; Jackson) and/or FITC-labelled horse anti-mouse (1:500; Vector) antibodies. For size-distribution studies, immunofluorescently stained sections double-labelled with anti-NeuN[29] were analysed using NIH image software. Glucose oxidase/nickel-enhanced diaminobenzidine immunostaining of spinal cord sections was performed using anti-VRL1 (0.83 $\mu g\,ml^{-1}$) as described[5].

Primary cultures prepared from adult rat DRG[30] were incubated overnight (37 °C, 5% CO_2) in medium containing nerve growth factor (100 $ng\,ml^{-1}$) and fixed with 10% formalin in 0.1 M phosphate buffer. For size-distribution studies, cells were stained with anti-VR1 or anti-VRL1 IgG (166 $ng\,ml^{-1}$), detected with diaminobenzidine–peroxidase (Vector), and analysed as above.

Received 9 November 1998; accepted 24 February 1999.

1. Dubner, R., Price, D. D., Beitel, R. E. & Hu, J. W. in *Pain in the Trigeminal Region* (eds Anderson, D. J. & Matthews, B.) 57–66 (Elsevier, Amsterdam, 1977).
2. Campbell, J. N. & Meyer, R. A. in *Spinal Afferent Processing* (ed. Yaksh, T. L.) 59–81 (Plenum, New York, 1986).
3. Leem, J. W., Willis, W. D. & Chung, J. M. Cutaneous sensory receptors in the rat foot. *J. Neurophysiol.* **69,** 1684–1699 (1993).
4. Caterina, M. J. *et al.* The capsaicin receptor: a heat-activated ion channel in the pain pathway. *Nature* **389,** 816–824 (1997).
5. Tominaga, M. *et al.* The cloned capsaicin receptor integrates multiple pain-producing stimuli. *Neuron* **21,** 531–543 (1998).
6. Montell, C. & Rubin, G. M. Molecular characterization of the *Drosophila trp* locus: a putative integral membrane protein required for phototransduction. *Neuron* **2,** 1313–1323 (1989).
7. Zhu, X. *et al. trp*, a novel mammalian gene family essential for agonist-activated capacitative Ca^{2+} entry. *Cell* **85,** 661–671 (1996).
8. Colbert, H. A., Smith, T. L. & Bargmann, C. I. Osm9, a novel protein with structural similarity to ion channels, is required for olfaction, mechanosensation and olfactory adaptation in *Caenorhabditis elegans*. *J. Neurosci.* **17,** 8259–8269 (1997).
9. Marsh, S. J., Stansfield, C. E., Brown, D. A., Davey, R. & McCarthy, D. The mechanism of action of capsaicin on sensory C-type neurons and their axons *in vitro*. *Neuroscience* **23,** 275–289 (1987).
10. Bevan, S. & Szolcsanyi, J. Sensory neuron-specific actions of capsaicin: mechanisms and applications. *Trends Pharmacol. Sci.* **11,** 330–333 (1990).
11. Winter, J., Walpole, C. S., Bevan, S. & James, I. F. Characterization of resiniferatoxin binding and capsaicin sensitivity in adult rat dorsal root ganglia. *Neuroscience* **57,** 747–757 (1993).
12. Bevan, S. *et al.* Capsazepine: a competitive antagonist of the sensory neuron excitant capsaicin. *Br. J. Pharmacol.* **107,** 544–552 (1992).
13. Dray, A., Forbes, C. A. & Burgess, G. M. Ruthenium red blocks the capsaicin-induced increase in intracellular calcium and activation of membrane currents in sensory neurones as well as the activation of peripheral nociceptors *in vitro*. *Neurosci. Lett.* **110,** 52–59 (1990).
14. Reuss, H., Mojet, M. H. Chyb, S. & Hardie, R. *In vivo* analysis of the *Drosophila* light-sensitive channels, TRP and TRPL. *Neuron* **19,** 1249–1259 (1997).
15. Meyer, R. A., Campbell, J. N. & Raja, S. in *Textbook of Pain* (eds Wall, P. D. & Melzack, R.) 13–44 (Churchill Livingstone, Edinburgh, 1994).
16. Helliwell, R. J. A. *et al.* Capsaicin sensitivity is associated with the expression of vanilloid (capsaicin) receptor (VR1) mRNA in adult rat sensory ganglia. *Neurosci. Lett.* **250,** 177–180 (1998).
17. Jancso, G., Kiraly, E. & Jancso-Gabor, A. Pharmacologically induced selective degeneration of chemosensitive primary sensory neurons. *Nature* **270,** 741–743 (1977).
18. Wood, J. N. *et al.* Capsaicin-induced ion fluxes in dorsal root ganglion cells in culture. *J. Neurosci.* **8,** 3208–3220 (1988).
19. Snider, W. D. & MacMahon, S. B. Tackling pain at the source: new ideas about nociceptors. *Neuron* **20,** 629–632 (1998).
20. McCarthy, P. W. & Lawson, S. N. Differing action potential shapes in rat dorsal root ganglion neurones related to their substance P and calcitonin gene-related peptide immunoreactivity. *J. Comp. Neurol.* **388,** 541–549 (1997).
21. Lawson, S. N. & Waddell, P. J. The antibody RT97 distinguishes between sensory cell bodies with myelinated and unmyelinated peripheral processes in the rat. *J. Physiol.* **371,** 59P (1985).
22. Wood, J. N. & Anderton, B. H. Monoclonal antibodies to mammalian neurofilaments. *Biosci. Rep.* **1,** 263–268 (1981).
23. Light, A. & Perl, E. R. Re-examination of the dorsal root projection to the spinal dorsal horn including observations on the differential termination of course and fine fibers. *J. Comp. Neurol.* **186,** 117–132 (1979).
24. Nagy, I. & Rang, H. Noxious heat activates all capsaicin-sensitive and also a subpopulation of capsaicin-insensitive dorsal root ganglion neurons. *Neuroscience* **88,** 995–997 (1999).
25. Hardie, R. C. & Minke, B. Novel Ca^{2+} channels underlying transduction in *Drosophila* hotoreceptors: implications for phosphoinositide-mediated Ca^{2+} mobilization. *Trends Neurosci.* **16,** 371–376 (1993).
26. Scott, K. & Zucker, C. TRP, TRPL and trouble in photoreceptor cells. *Curr. Opin. Neurobiol.* **8,** 383–388 (1998).
27. Nathans, J. Molecular biology of visual pigments. *Annu. Rev. Neurosci.* **10,** 163–194 (1987).
28. Brake, A., Wagenbach, M. J. & Julius, D. New structural motif for ligand-gated ion channels defined by an ionotropic ATP receptor. *Nature* **371,** 519–523 (1994).
29. Todd, A. J., Spike, R. C. & Polgar, E. A quantitative study of neurons which express neurokinin-1 or somatostatin sst2a receptor in rat spinal cord dorsal horn. *Neuroscience* **85,** 459–473 (1998).
30. Reichling, D. B. & Levine, J. D. Heat transduction in rat sensory neurons by calcium-dependent activation of a cation channel. *Proc. Natl Acad. Sci. USA* **94,** 7006–7011 (1997).

Acknowledgements. We thank M. Bland for assistance with immunolocalization; L. England, J. Onuffer and members of the Basbaum laboratory for advice regarding primary neuronal culture, immunolocalization, and affinity purification methods; and A. Basbaum, H. Chuang, L. England, H. Ingraham and S. Jordt for comments on the manuscript. M.J.C. is an American Cancer Society postdoctoral fellow and NARSAD young investigator; M.T. is a Comroe Fellow of the UCSF Cardiovascular Research Institute. This work was supported by grants from NIGMS and NIDR.

Correspondence and requests for materials should be addressed to D.J. (e-mail: julius@socrates.ucsf.edu). The Genbank accession numbers for rat and human VRL-1 cDNAs are AF129113 and AF129112, respectively.

Prisoner's dilemma in an RNA virus

Paul E. Turner* & Lin Chao*

Department of Biology, University of Maryland, College Park, Maryland 20742, USA

The evolution of competitive interactions among viruses[1] was studied in the RNA phage φ6 at high and low multiplicities of infection (that is, at high and low ratios of infecting phage to host cells). At high multiplicities, many phage infect and reproduce in the same host cell, whereas at low multiplicities the viruses reproduce mainly as clones. An unexpected result of this study[1] was that phage grown at high rates of co-infection increased in fitness initially, but then evolved lowered fitness. Here we show that the fitness of the high-multiplicity phage relative to their ancestors generates a pay-off matrix conforming to the prisoner's dilemma strategy of game theory[2,3]. In this strategy, defection (selfishness) evolves, despite the greater fitness pay-off that would result if all players were to cooperate. Viral cooperation and defection can be defined as, respectively, the manufacturing and sequestering of diffusible (shared) intracellular products. Because the low-multiplicity phage did not evolve lowered fitness, we attribute the evolution of selfishness to the lack of clonal structure and the mixing of unrelated genotypes at high multiplicity[4–6].

Evolutionary game theory predicts the outcome of pairwise contests between players that use conflicting strategies[3]. If a population of individuals playing one strategy cannot be invaded by mutants playing any other strategy, the former becomes the evolutionarily stable strategy. But if no single strategy is able to resist invaders, a polymorphic equilibrium with both strategies ensues. Whether a single strategy or a polymorphic equilibrium evolves depends on the fitness pay-offs to the players. In a contest between the strategies of cooperation and defection, the resulting 2×2 pay-off matrix is described by three variables (Fig. 1a). When a pair of cooperators interact, their individual fitness has a value of one. When a cooperator and a defector are paired, the cooperator is exploited and its fitness is decreased by s_1, whereas the defector benefits and its fitness is increased by s_2. When two defectors interact, they suffer from not having anyone to exploit and pay a cost c. If $(1 - c) < (1 - s_1)$ a polymorphic equilibrium results. If $(1 - c) > (1 - s_1)$ the population evolves to be 100% defectors. The latter is evolutionarily paradoxical, and termed the prisoner's dilemma, because a population composed of defectors has a lower fitness than one containing only cooperators. Although the prisoner's dilemma is clearly of evolutionary importance, it is difficult in most biological systems to measure the pay-off values associated with it[7–9] and most examples are theoretical[10].

Viral evolution offers a unique opportunity to study the prisoner's dilemma because co-infection of the same host cell by more than one virus creates conflicts[1,11–13] similar to those assumed in game theory, and ancestral genotypes can often be retrieved for reconstructing the pay-off matrix. The manufacture of diffusible and hence shared intracellular products by viruses co-infecting the same cell allows for the strategies of cooperation and defection. A viral genotype that synthesizes larger quantities of products is effectively a cooperator. In contrast, a genotype that synthesizes less but specializes in sequestering a larger share of the products is a defector. The often observed evolution of defective interfering particles[14] in viruses supports this interpretation. The particles are coded by viral RNAs that have lost most or all of their protein-coding sequences,

* Present addresses: Instituto Cavanilles de Biodiversidad y Biología Evolutiva and Departamento de Genética, Universidad de Valéncia, 46100 Valéncia, Spain (P.E.T.); and Department of Biology, University of California San Diego, La Jolla, California 92093-0116, USA (L.C.).